Photocatalytic Activity and Filtration Performance of Hybrid TiO2-Cellulose Acetate Nanofibers for Air Filter Applications

Miyeon Kwon
KITECH: Korea Institute of Industrial Technology
Juran Kim (jkim0106@kitech.re.kr)
Korea Institute of Industrial Technology

Research Article

Keywords: nanofibers, Tio2-CA, air filters

Posted Date: March 11th, 2021

DOI: https://doi.org/10.21203/rs.3.rs-276494/v1

Abstract

A facile method to prepare hybrid cellulose acetate nanofibers containing TiO_2 (TiO_2 -CA nanofiber) by emulsion electrospinning technique was developed for denitrification and the filtration of particulate matters (PMs). This work found that hybrid TiO_2-CA nanofibers mainly contain the anatase form of TiO_2, attributing to the photodecomposition of NO gas under UV irradiation. TiO_2-CA nanofibers also showed excellent filtration efficiency of 99.5% for $PM_{0.5}$ and photocatalytic efficiency of 78.6% for NO removal. Furthermore, the results implied the morphology of TiO_2-CA nanofibers, such as micro-wrinkles and protrusions, increased the surface hydrophobicity up to 140° with increased addition of TiO_2 nanoparticles. The proposed TiO_2-CA nanofibers, as a result, would be promising materials of highly efficient and sustainable air filters for industrial and home appliance systems.

Introduction

Air pollution is a serious environmental issue that is continuously burdening our daily life. In general, the most concerning air pollutants are sulfur dioxide (SO_2), nitrogen oxides (NO and NO_2), volatile organic compounds (VOCs), particulate matters (PMs), carbon monoxide (CO), carbon dioxide (CO_2), ozone, chlorofluorocarbons and trace heavy metals (Lelieveld et al. 2015). Among air pollutants, PMs are comprised of a complex mixture of sulfate, nitrates, ammonia, sodium chloride, carbon black, mineral dusts, and water. Depending on their sizes, PMs can be classified as $PM_{0.5}$, $PM_{2.5}$ and PM_{10}, which denote to particle sizes below 0.5, 2.5 and 10 μm, respectively. These PMs are very detrimental to human health since they can penetrate human bronchi and lungs to cause chronic pulmonary disease and lung cancer (Xiang et al. 2019). In 2013, the World Health Organization also reported that air pollutants such as PMs are carcinogens to humans and can even induce death (Zhang et al. 2019).

For a few years, the photocatalytic activities have been well studied to remove various pollutants such as PMs, SO_2, NO, NO_2, and various VOCs in the air environment (Su et al. 2013). Particularly, photocatalytic degradation using titanium dioxide (TiO_2) is one of the most generally studied methods because it powerfully converts rich solar energy into active chemical energy that can decompose harmful pollutants in the air (Lee et al. 2009). TiO_2 excites electrons under UV illumination from the valence band to the conduction band and leaves holes in the valence band. At that moment, the electrons change oxygen molecules to superoxide anions and the holes react with water molecules in the air to produce hydroxyl radicals. These two species, superoxide anions and hydroxyl radicals, are very reactive and capable of decomposing air pollutants such as PMs, SO_2, NO, NO_2 and VOCs. (Fujishima and Honda 1972).

Several TiO_2 incorporated nanofibers have been of great interest for the removal of air pollutants because of their well-defined dimensions, high specific surface areas, and greater photocatalytic activities (Fallah et al. 2018; Khan et al. 2015; Lin et al. 2019). For example, polyacrylonitrile (PAN) nanofibers with embedded commercial photocatalysts, P25 and TiO_2 particles, showed an excellent filtration efficiency of 96.75% for $PM_{2.5}$ (Chen et al. 2019). Dong et al. have studied about the effective strategy for in situ

growth of high adhesion of TiO_2 to polyvinylidene fluoride (PVDF) nanofibers via electrospinning coupled with cold plasma pretreatment and hydrothermal processing (Dong et al. 2019). On the other hand, bamboo cellulose acetate fibers grafted with TiO_2 have presented photocatalytic ability to decompose phenol under UV illumination (Lu et al. 2013). Lastly, electrospun TiO_2 entrapped-chitosan hybrid nanofibers were developed for the removal of heavy metal ions (Razzaz et al. 2016).

However, there is a major problem that restricts the application of photocatalytic fiber using TiO_2. First is the brittleness of TiO_2 incorporated nanofibers. Li et al. have reported about the brittle polycrystalline TiO_2-incorporated nanofibers produced from a precursor solution such as titanium alkoxide ($Ti(OR)_4$) with poly(vinyl pyrrolidone), leading to reduced photocatalytic activities until after calcination (Li and Xia 2003). Another problem is that studies on the application of TiO_2-incorporated nanofibers and their photocatalytic activities for simultaneous denitrification have not been sufficient thus far. The weak adhesion between TiO_2 and the polymeric nanofibers is also a key obstacle that inhibits their practicability. Moreover, the high photocatalytic activity of TiO_2-incorporated nanofibers without the degradation of polymeric substrates still remains a critical challenge.

In order to overcome these drawbacks of TiO_2-incorporated nanofiber applications, there is a call for a detailed investigation of the photocatalytic effects of TiO_2-incorporated into nanofibers for the removal of air pollutants, In this study, we present a fast and facile fabrication method of hybrid cellulose acetate nanofibers containing TiO_2 (TiO_2-CA nanofibers) using by emulsion electrospinning and evaluate the photodecomposition of nitrogen oxides under UV illumination as well as filtration efficiency.

Materials And Methods

Materials

Titanium isopropoxide (TTIP), cellulose acetate anhydrous sodium sulfate (CA, Mn = 30,000 Da, the degree of acetylation: 39.3–40.3 wt%), isopropyl alcohol (> 99.7% grade), acetone, N,N-dimethylacetamide, NaOH (0.1 M in water), and acetone were purchased from Sigma Aldrich Co., LLC, Korea (Seoul, Korea).

Synthesis of TiO_2 nanoparticles

10 mL of the titanium isopropoxide (TTIP) as a precursor was mixed with 40 mL isopropyl alcohol and stirred for 30 min. Then 10 mL of a mixture (1:1) of deionized water and isopropyl alcohol was added drop gradually into the TTIP mixture to form a colloidal solution under vigorous stirring. The pH of the obtained colloidal solution was adjusted using NaOH solution and irradiated by sonication (Power sonic 510, Seoul, South Korea) at 40 kHz for 30 min. The colloidal solution was dried in an oven at 110°C for 3 h and TiO_2 nanoparticles were calcinated at 400 C° for 1 h.

Fabrication of TiO_2-CA nanofiber webs

TiO_2-CA nanofibers were fabricated using emulsion electrospinning. First, 10 wt% CA pellets were dissolved in a mixture of N,N-dimethylacetamide and acetone at the ratio of 1:2 (v/v). The solution was then stirred at 500 rpm and room temperature for 5 h. Afterwards, 5 or 10 wt% of synthesized TiO_2 nanoparticles of CA pellets were put into the CA solution. To evenly disperse TiO_2 nanoparticles in CA solutions, sonication (Power sonic 510, Seoul, South Korea) was employed at 40 kHz for 30 min. The solution was put into a 15 mL syringe and electrospun at a feeding rate of 1 mL h^{-1}. The distance between the taylor cone and the collector was 15 cm and 18 kV was applied for the fabrication of TiO_2-CA nanofiber webs.

Characteristics of synthesized TiO_2 nanoparticles and TiO_2-CA nanofibers

X-ray diffractometer (XRD, D8 Advance, Bruker, USA) was performed to analyze crystalline phases of the synthesized TiO_2 nanoparticles and TiO_2-CA nanofibers. XRD was operated in reflection mode with Cu-K radiation (35 kV, 30 mA) and diffracted beam monochromator, using a step scan mode with the step of 0.075° and 4 s per step. Diffraction patterns of both anatase and rutile TiO_2 powders were compared with reference to the JCPDS database.

Contact angle measurement and morphology of TiO_2-CA nanofiber webs

The contact angle of TiO_2-CA nanofiber webs was measured using a contact angle goniometer (DSA 25, Kruss, Matthews, USA) and the sessile drop technique at room temperature. 10 µL of deionized water (γ_{LV} = 72.8 mN/m) droplet was deposited on CA and TiO_2-CA nanofiber webs using a syringe and the measurement was repeated at least five times in order to analyze the hydrophobicity of TiO_2-CA nanofiber webs. Additionally, the morphology and average diameter of TiO_2 nanoparticles, untreated CA nanofibers and TiO_2-CA nanofibers were analyzed by scanning electron microscopy (SEM, Hitachi, Tokyo, Japan) with an energy dispersive X-ray analyzer (EDX) to evaluate the atom weight percent on the surface of TiO_2-CA nanofibers.

Photocatalytic activity of TiO_2-CA nanofiber webs for NO removal

The photocatalytic activities of TiO_2-CA nanofiber webs were evaluated based on ISO 22197-1:2016 for the removal of NO gas. TiO_2-CA nanofiber or untreated CA nanofiber (5 cm × 10 cm) samples were placed in the middle of two plain glasses (5 cm × 10 cm) of non-photocatalytic blank samples in the photoreactor. A UV lamp system was placed over the photoreactor, delivered a UVA irradiance (10 W m^{-2}) from 2 × 6 W BLB lamps with a 365 nm emission peak. All three samples were illuminated with UV light. NO_x analyzer (T-API, T200, San Diego, USA) was used to measure nitrate concentrations every 1 min. NO gas flowed at a rate of 3 L min^{-1} containing 1 ppm_v of NO in air with 50% of relative humidity at 25°C under UV light. The concentration of NO in the outlet stream was monitored for 20 min. before the light was switched on, and then during the 1 h UV irradiation.

Filtration efficiency of TiO_2-CA nanofiber webs

For filtration efficiency, TiO_2-CA nanofiber webs were measured using the TSI-3160 filter tester (TSI Inc., Shoreview, MN, USA). In this system, sodium chloride particles were used as representative PMs. This tester was able to generate sodium chloride nanoparticles with sizes ranging between 100 and 600 nm in the flowing air. measuring particle penetration versus particle size at 32.28 L min^{-1} aerosol flow rate and 5.38 cm s^{-1} face velocity. TiO_2-CA nanofiber webs were placed at the bottom of a sample holder on a wide-mesh metal net to support the specimen. The % penetration of sodium chloride particles passing through the TiO_2-CA nanofiber webs was determined by the relative particle concentration upstream and downstream of the sample (Zhai and Jana 2017).

Results And Discussion

The morphology of TiO_2 and TiO_2-CA nanofibers

Figure 1 shows the morphology of synthesized TiO_2 nanoparticles that display irregular shape and rough surface without pore. The diameters of TiO_2 nanoparticles were measured from randomly selected areas of SEM images using Nahwoo imaging software ($N \geq 100$) (Iworks 2.0, Suwon, South Korea). The average diameter of TiO_2 nanoparticles was 54 nm (± 5.6).

As shown in Fig. 2, untreated CA nanofibers have smooth surfaces and no defects. The average diameter size of CA nanofibers is 278 nm with a standard deviation of 78 nm; however, TiO_2-CA nanofibers display increasing roughness and average diameter size with the addition of TiO_2 loadings. CA nanofibers containing 5 or 10 wt% TiO_2 induce the formation of abnormal beads on the surface that result in uneven morphology and micro-wrinkles (Lee et al. 2016). During electrospinning, a highly volatile solvent can solidify immediately on the surface of the nanofibers while the fluid jet is flying to the collector, whereby it becomes hard for the nanoparticles to be transferred from the core to the shell of the nanofibers (Ding et al. 2011). Compared to the diameter range of 5 wt% TiO_2-CA nanofibers from 200 to 1050 nm, the average diameter of TiO_2-CA nanofibers is 378 nm ($\sigma = 74$) as shown in Fig. 2(c and d). Figure 2(e) highlights the 454 nm ($\sigma = 126$) average diameter of 10 wt% TiO_2-CA nanofibers, lying within the 150 to 1300 nm diameter range of 10 wt% TiO_2-CA nanofibers. The rough surface and grafted TiO2 nanoparticles are shown in Figure. 2 (g and h). In Fig. 2(b and f), the quantitative analyses of each untreated CA nanofibers element and 5 and 10 wt% TiO_2-CA nanofibers are compared through an energy dispersive X-ray analyzer (EDX, attached to the SEM). The data show spectra with peaks corresponding to all the different elements. In Table 1, the EDX data show each element concentration percentage of different samples. For 5 wt% TiO_2-CA nanofibers, carbon and oxygen atoms mainly occupied 47.1 wt% and 46.7 wt% of the sample, respectively. Untreated CA nanofibers exhibit no Ti content on surface. In contrast, 5 and 10 wt% TiO_2-CA nanofibers comprise of 6.3% and 11.6 wt% Ti on surface, respectively.

From the data, we confirmed that the final TiO_2-CA nanofibers maintained a similar weight to the initial addition of TiO_2.

XRD analysis of TiO_2 nanoparticles and TiO_2-CA nanofibers

Both anatase and rutile are well-known as stable phases of TiO_2 nanoparticles (Fallah et al. 2018). TiO_2 nanoparticles are most likely to be a mixture of those phases rather than pure anatase or rutile; therefore, quantitative analysis is highly important. Figure 3 and Table 2 show the XRD patterns of synthesized TiO_2 nanoparticles and TiO_2-CA nanofibers in the 2θ range of 10–70° according to standard JCPDS card No. 21-1272. The anatase reflections dominated the reflection patterns while rutile was present as well. All diffraction peaks at 25.25°, 37.80°, 38.50°, 48.05°, 53.9°, 55.05°, 62.65°, 68.85°, 70.30°, 75.05° and 76.10° were well indexed as pure anatase phases. Rutile phases showed diffraction peaks at 27°, 36° and 55°, the crystalline region of TiO_2 (Ananpattarachai et al. 2009). For 5 or 10 wt% TiO_2-CA nanofibers, the new diffraction peaks at 22.6° mainly represented the crystalline region of the cellulose (Li et al. 2011; Lu et al. 2013). From the XRD analysis, the results show that crystalline TiO_2 nanoparticles consisted of 87.8 % of anatase and 12.7% of rutile forms and TiO_2-CA nanofibers contained both anatase and rutile forms of TiO_2 nanoparticles after fabrication.

Table 1
Quantitative analysis of untreated CA and TiO_2-CA nanofibers

Materials	**5 wt% TiO_2-CA nanofibers**		**10 wt% TiO_2-CA nanofibers**		**Untreated CA nanofibers**	
Element	Weight %	Atom %	Weight %	Atom %	Atom %	Atom %
C	47.1	56.2	42.7	53.4	49.5	56.6
O	46.7	41.9	45.7	42.9	50.5	43.4
Ti	6.3	1.9	11.6	3.6	-	-

Table 2
XRD analysis of synthesized TiO_2 nanoparticles and TiO_2-CA nanofibers

	Compound	**2θ (degree)**
TiO_2 Nanoparticles	Anatase	25.25°, 37.80°, 38.50°, 48.05°, 53.9°, 55.05°, 62.65°
	Rutile	27°, 36° and 55°
TiO_2-CA nanofibers	Cellulose	22.6°
	Anatase	25.25°, 37.80°, 38.50°, 48.05°, 53.9°, 55.05°
	Rutile	27°, 36° and 55°

The photocatalytic effect of NO removal

In order to confirm the inevitability of UV irradiation for photocatalytic reaction, the tests of UV irradiation (turning on UV lamp) and darkness (turning off UV lamp) for denitrification were carried out, as exhibited in Fig. 4.

The results show that the NO removal efficiency changes greatly with or without UV irradiation. Specifically, the denitrification efficiency in the dark was less than 0.1%, mainly due to the physical adsorption of NO over TiO_2-CA nanofibers. After turning on the UV light for 60 min, the NO removal efficiency of 5 or 10 wt% TiO_2-CA nanofibers showed a rapid upward trend and increased to 64.5% and 78.6%, respectively. Untreated CA nanofibers, however, showed no effect with or without UV light.

When the UV light was turned off, the removal efficiency of NO decreased rapidly due to the initial adsorption equilibrium level in the dark. This implies that there is a significant effect of UV irradiation on NO removal, meaning that UV light is an vital factor in the photocatalytic reaction of NO gas removal.

The filtration efficiency of TiO_2-CA nanofiber webs

Various sizes of PMs were tested for filtration efficiencies of 10 wt% TiO_2-CA nanofiber webs. Figure 5(a) shows filtration efficiency (%) and air penetration (%) of 10 wt% TiO_2-CA nanofibers depending on NaCl particle size. Clearly, the filtration efficiencies against all size PMs were higher than 97%. TiO_2-CA nanofiber webs showed increased efficiencies from 97.1 to 99.6 % in particle sizes 0.1 ($PM_{0.1}$) to 0.6 μm ($PM_{0.6}$). However, air penetration decreased from 2.93 to 0.42 %. The pressure drop was consistently near 3.13 mmH_2O for most particle sizes.

SEM images of 10 wt% TiO_2-CA nanofibers after capturing NaCl nanoparticles (represented as PMs) are shown in Fig. 5(b). 0.1–0.6 μm sized PMs were captured at the surface and around nanofibers, revealing a strong electrostatic force present at the surface of 10 wt% TiO_2-CA nanofibers that attracts PMs that are much smaller than the thru-holes because of the electrostatic force created by air flow friction. A study on the electrosurface properties and interaction of cellulose nanofibers and TiO_2 nanoparticles stated that the cellulose nanofibers and titanium dioxide nanoparticles attracted to one another due to electrostatic forces on the surface (Martakov et al. 2018).

Contact angle analysis

The hydrophobicity of untreated CA or TiO_2-CA nanofiber webs was subsequently measured, with the results of water contact angle measurements on different samples illustrated in Fig. 6. In all membranes incorporated with TiO_2 nanoparticles, the value of the contact angles increased with the addition of TiO_2 loadings. To be specific, the contact angle of untreated CA nanofibers was 112.5° while that of TiO_2-CA nanofibers increased from 127.8° to 140° with an addition of TiO_2 nanoparticles. When TiO_2 nanoparticles were incorporated with CA nanofibers, the hydrophobicity of TiO_2-CA nanofibers saw improved due to surface roughness as shown in Fig. 2 (g and h). This supports previous research around improved surface hydrophobicity that stems from morphology traits such as micro-wrinkles and

protrusions of nanofibers through the mitigation of wetting and decreasing water-membrane contact area (Liao et al. 2014). Guan has also studied the relationship between hydrophilicity and photocatalytic activity: the surface with more hydrophilicity resulted in less photocatalytic activity (Guan 2005).

Conclusions

In this study, we have shown a facile and efficient fabrication method to prepare hybrid TiO_2-CA nanofibers for photocatalytic activity of denitrification and improved filtration of PMs. The photocatalytic effects of TiO_2-CA nanofibers denitrification decomposed NO gas up to 78.6%. A single-layer TiO_2-CA nanofiber webs effectively filtered and captured PMs (0.1–0.6 μm) up to 99.6%. As a result, this investigation demonstrates a novel method to fabricate TiO_2-CA nanofibers and utilize its highly photocatalytic efficiency to a wide range of potential applications including protective clothing systems, sensors, industrial and home appliance filtration systems, and much more.

Declarations

Acknowledgment

This research was supported by the R&D Program of Ministry of Culture, Sports and Tourism and the Korea Creative Content Agency of Republic of Korea (Development of nature friendly media art platform for enjoyment of culture and art on forest and park, R2019020020).

Conflicts of interest

The authors declare no conflict of interest.

References

Ananpattarachai J, Kajitvichyanukul P, Seraphin S (2009) Visible light absorption ability and photocatalytic oxidation activity of various interstitial N-doped TiO2 prepared from different nitrogen dopants Journal of Hazardous Materials 168:253-261 doi:https://doi.org/10.1016/j.jhazmat.2009.02.036

Chen K-N, Sari FNI, Ting J-M (2019) Multifunctional TiO2/polyacrylonitrile nanofibers for high efficiency PM2.5 capture, UV filter, and anti-bacteria activity Applied Surface Science 493:157-164 doi:https://doi.org/10.1016/j.apsusc.2019.07.020

Ding B, Lin J, Wang X, Yu J, Yang J, Cai Y (2011) Investigation of silica nanoparticle distribution in nanoporous polystyrene fibers Soft Matter 7:8376-8383 doi:10.1039/C1SM05791J

Dong P, Huang Z, Nie X, Cheng X, Jin Z, Zhang X (2019) Plasma enhanced decoration of nc-TiO2 on electrospun PVDF fibers for photocatalytic application Materials Research Bulletin 111:102-112 doi:https://doi.org/10.1016/j.materresbull.2018.11.007

Fallah Z, Nasr Isfahani H, Tajbakhsh M, Tashakkorian H, Amouei A (2018) TiO2-grafted cellulose via click reaction: an efficient heavy metal ions bioadsorbent from aqueous solutions Cellulose 25:639-660 doi:10.1007/s10570-017-1563-8

Fujishima A, Honda K (1972) Electrochemical Photolysis of Water at a Semiconductor Electrode Nature 238:37-38 doi:10.1038/238037a0

Guan K (2005) Relationship between photocatalytic activity, hydrophilicity and self-cleaning effect of TiO2/SiO2 films Surface and Coatings Technology 191:155-160 doi:https://doi.org/10.1016/j.surfcoat.2004.02.022

Khan S, Ul-Islam M, Khattak WA, Ullah MW, Park JK (2015) Bacterial cellulose-titanium dioxide nanocomposites: nanostructural characteristics, antibacterial mechanism, and biocompatibility Cellulose 22:565-579 doi:10.1007/s10570-014-0528-4

Lee E-J, An AK, He T, Woo YC, Shon HK (2016) Electrospun nanofiber membranes incorporating fluorosilane-coated TiO2 nanocomposite for direct contact membrane distillation Journal of Membrane Science 520:145-154 doi:https://doi.org/10.1016/j.memsci.2016.07.019

Lee JA, Krogman KC, Ma M, Hill RM, Hammond PT, Rutledge GC (2009) Highly Reactive Multilayer-Assembled TiO2 Coating on Electrospun Polymer Nanofibers Advanced Materials 21:1252-1256 doi:https://doi.org/10.1002/adma.200802458

Lelieveld J, Evans JS, Fnais M, Giannadaki D, Pozzer A (2015) The contribution of outdoor air pollution sources to premature mortality on a global scale Nature 525:367-371 doi:10.1038/nature15371

Li D, Xia Y (2003) Fabrication of Titania Nanofibers by Electrospinning Nano Letters 3:555-560 doi:10.1021/nl034039o

Li J, Lu Y, Yang D, Sun Q, Liu Y, Zhao H (2011) Lignocellulose Aerogel from Wood-Ionic Liquid Solution (1-Allyl-3-methylimidazolium Chloride) under Freezing and Thawing Conditions Biomacromolecules 12:1860-1867 doi:10.1021/bm200205z

Liao Y, Wang R, Fane AG (2014) Fabrication of Bioinspired Composite Nanofiber Membranes with Robust Superhydrophobicity for Direct Contact Membrane Distillation Environmental Science & Technology 48:6335-6341 doi:10.1021/es405795s

Lin Z, Lu Y, Huang J (2019) A hierarchical Ag2O-nanoparticle/TiO2-nanotube composite derived from natural cellulose substance with enhanced photocatalytic performance Cellulose 26:6683-6700 doi:10.1007/s10570-019-02573-z

Lu Y, Sun Q, Liu T, Yang D, Liu Y, Li J (2013) Fabrication, characterization and photocatalytic properties of millimeter-long TiO2 fiber with nanostructures using cellulose fiber as a template Journal of Alloys and Compounds 577:569-574 doi:https://doi.org/10.1016/j.jallcom.2013.06.183

Martakov IS, Torlopov MA, Mikhaylov VI, Krivoshapkina EF, Silant'ev VE, Krivoshapkin PV (2018) Interaction of cellulose nanocrystals with titanium dioxide and peculiarities of hybrid structures formation Journal of Sol-Gel Science and Technology 88:13-21 doi:10.1007/s10971-017-4447-3

Razzaz A, Ghorban S, Hosayni L, Irani M, Aliabadi M (2016) Chitosan nanofibers functionalized by TiO2 nanoparticles for the removal of heavy metal ions Journal of the Taiwan Institute of Chemical Engineers 58:333-343 doi:https://doi.org/10.1016/j.jtice.2015.06.003

Su C, Ran X, Hu J, Shao C (2013) Photocatalytic Process of Simultaneous Desulfurization and Denitrification of Flue Gas by TiO2–Polyacrylonitrile Nanofibers Environmental Science & Technology 47:11562-11568 doi:10.1021/es4025595

Xiang J et al. (2019) Reducing Indoor Levels of "Outdoor PM2.5" in Urban China: Impact on Mortalities Environmental Science & Technology 53:3119-3127 doi:10.1021/acs.est.8b06878

Zhai C, Jana SC (2017) Tuning Porous Networks in Polyimide Aerogels for Airborne Nanoparticle Filtration ACS Applied Materials & Interfaces 9:30074-30082 doi:10.1021/acsami.7b09345

Zhang T, Zhao Y, Bai H, Liu Y, Liu Y, Zhang Q (2019) Efficient As(III) removal directly as basic iron arsenite by in-situ generated Fe(III) hydroxide from ferrous sulfate on the surface of CaCO3 Applied Surface Science 493:569-576 doi:https://doi.org/10.1016/j.apsusc.2019.07.048

Figures

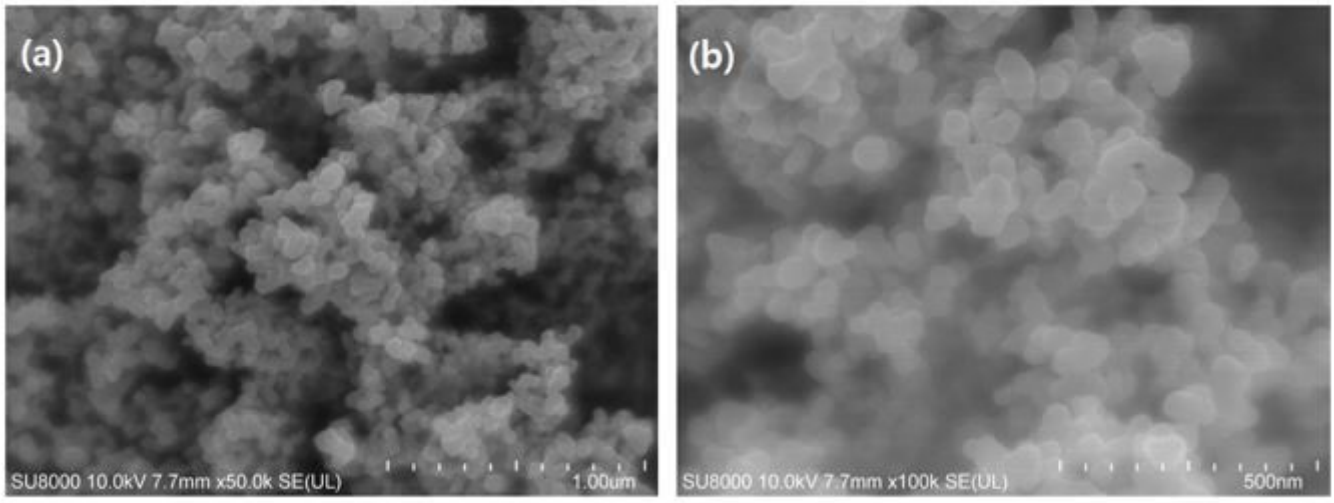

Figure 1

The morphology of synthesized TiO2 nanoparticles

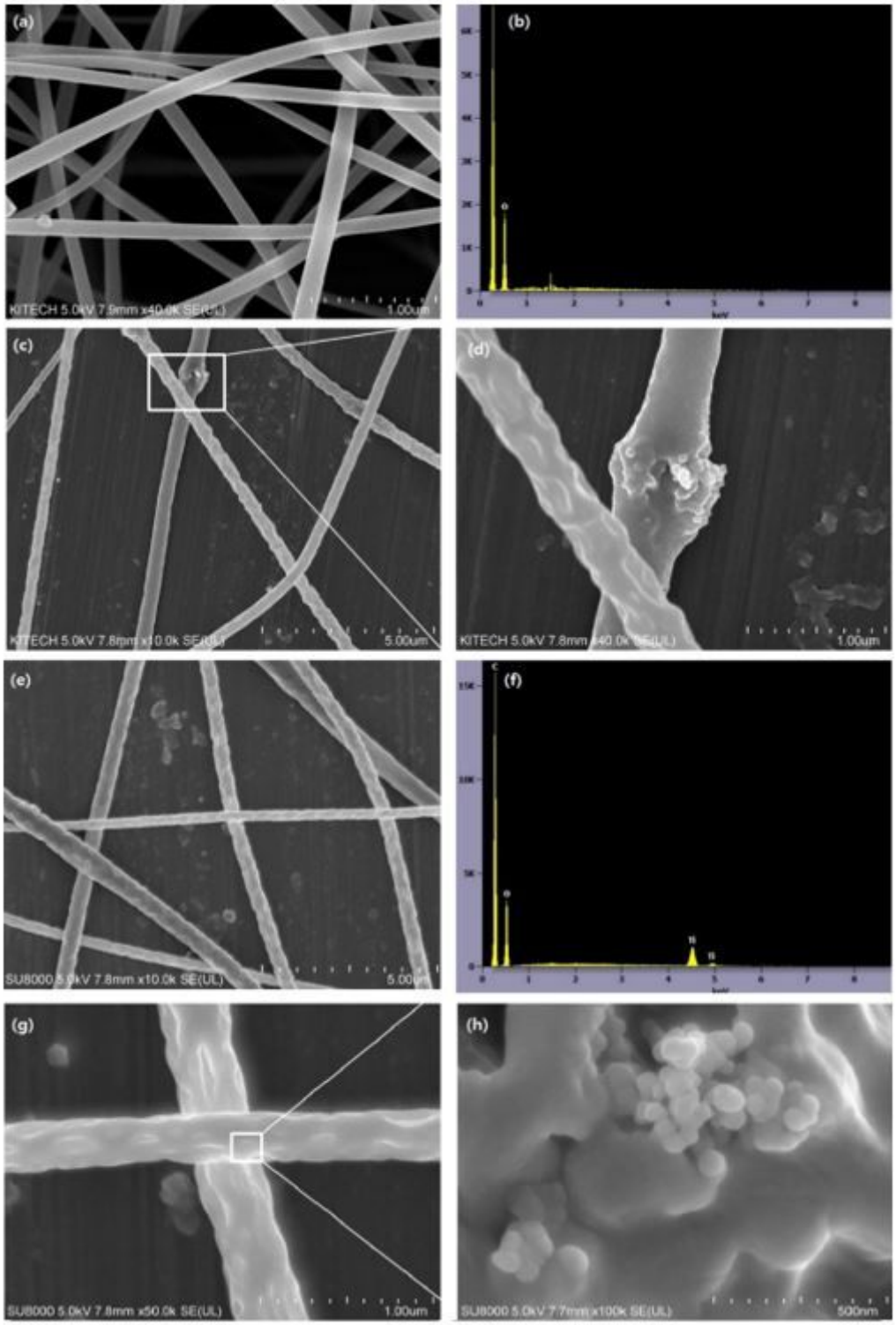

Figure 2

SEM images of (a) untreated CA nanofibers, (b) EDX analysis of untreated CA nanofibers, (c and d) 5 wt% TiO2-CA nanofibers, (e) 10 wt% TiO2-CA nanofibers, (f) EDX analysis of 10 wt% TiO2-CA and (g and h) the surface morphology of 10 wt% TiO2-CA nanofibers

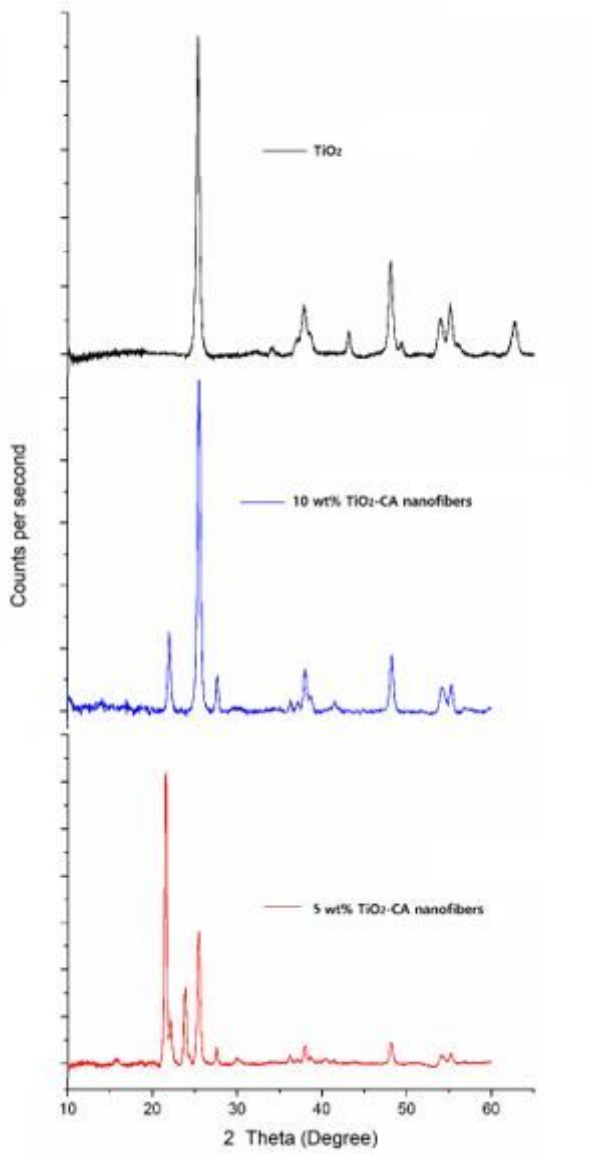

Figure 3

XRD patterns of synthesized TiO2 nanoparticles, 5 and 10 wt% TiO2-CA nanofibers.

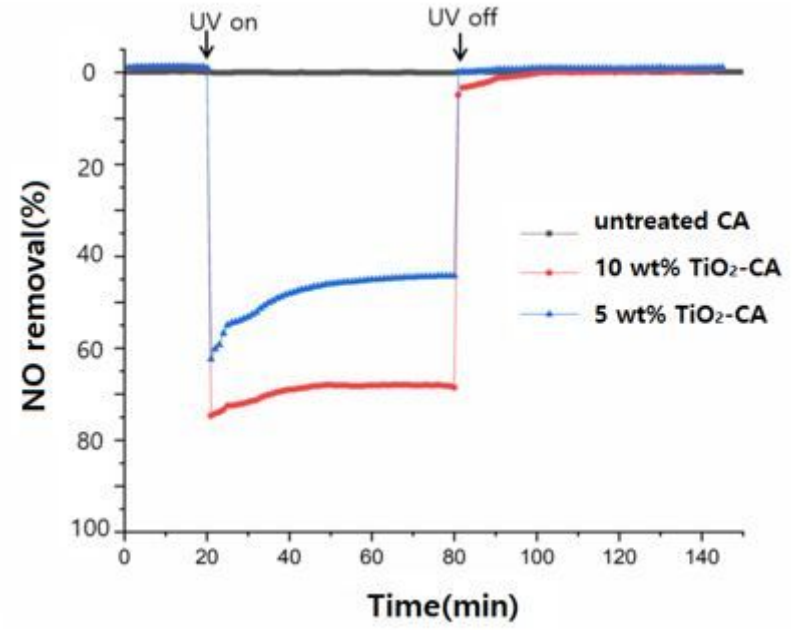

Figure 4

The photocatalytic effect of TiO2-CA nanofibers for NO gas removal

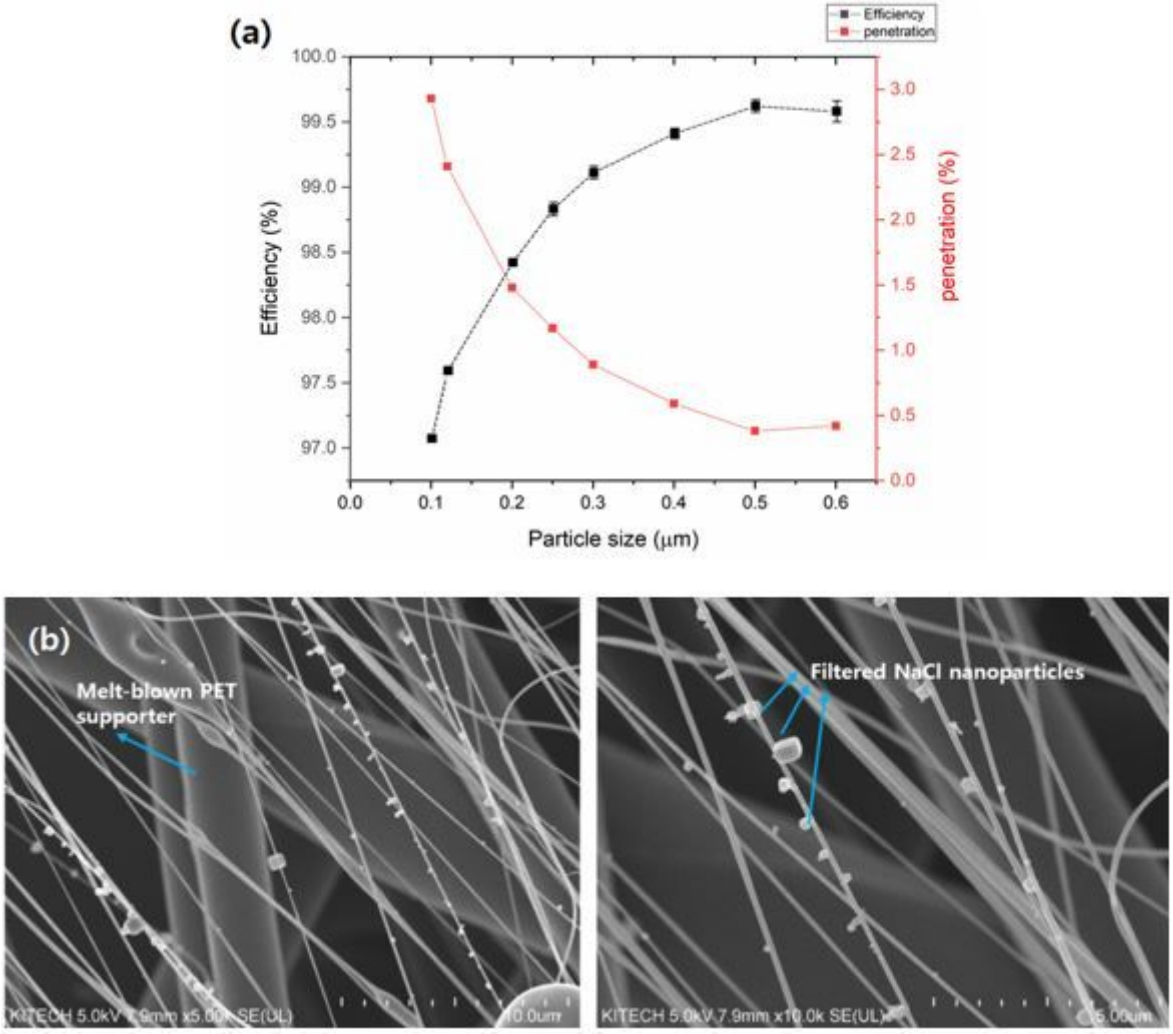

Figure 5

(a) Diagrams of the filtration efficiency (%) and air penetration (%) of 10 wt% TiO2-CA nanofiber webs and (b) captured NaCl particles (represented as PMs) on TiO2-CA nanofibers

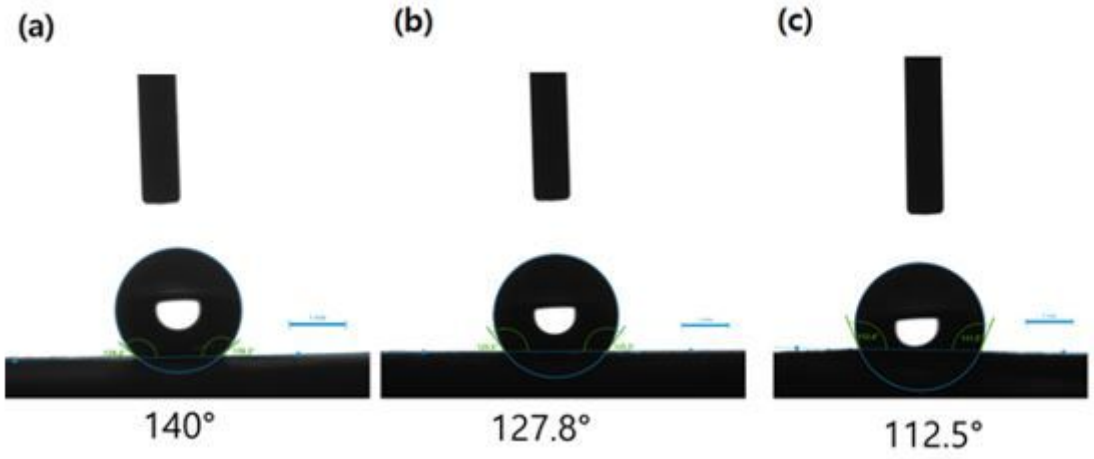

Figure 6

Contact angles of (a) 10 wt% TiO2-CA nanofibers, (b) 5 wt% TiO2-CA nanofibers and (c) untreated CA nanofibers